Supplementary Information

Indoor Burning of Arabian Incense Generates Ultrafine-Rich Particles with Strong Oxidative Potential

Liyuan Zhou[1,2*], Zhancong Liang[2], Wei Xu[1], Ru-Jin Huang[3], Patrick K. H. Lee[4] and Chak K. Chan[2*]

[1]State Key Laboratory of Advanced Environmental Technology, Institute of Urban Environment, Chinese Academy of Sciences, Xiamen 361021, China

[2]Division of Biological and Environmental Science and Engineering, King Abdullah University of Science and Technology, Thuwal, Jeddah 23955-6900, Kingdom of Saudi Arabia

[3]State Key Laboratory of Loess Science, Institute of Earth Environment, Chinese Academy of Sciences, Xi'an 710061, China

[4]School of Energy and Environment, City University of Hong Kong, Hong Kong SAR, China

Correspondence to: Liyuan Zhou (lyzhou@iue.ac.cn) and Chak K. Chan (chak.chan@kaust.edu.sa)

Contents

Figure S11. Elemental-class signal contributions partitioned by AImod for Bakhoor burning (mean of Types 1–3) and sidestream cigarette smoke particle extracts.

Figure S12. Change in OP_{DTTm} after Chelex treatment of water extracts from Bakhoor burning and sidestream cigarette smoke particles.

Figure S13. MTT-based cell viability as a function of particle mass loading for Bakhoor burning and sidestream cigarette smoke particles.

Figure S14. Size-resolved LDSA and regional (Tb/Al) LDSA contributions for Bakhoor burning versus sidestream cigarette smoke particles.

Figure S15. Ratios of mass-normalized and emission-weighted DTT-based oxidative potential for treated (wood-residue, tissue-wiped) versus untreated Bakhoor burning particles.

Text S1. Calculation of the modified aromaticity index (AI_{mod}).

For ultra-high-performance liquid chromatography coupled with high-resolution Orbitrap mass spectrometry data, elemental formulas were assigned to detected peaks. Only peaks meeting the signal-to-noise criterion used in this work were considered, and formula assignment was performed with the maximum mass error limited to ±3 ppm. Assigned compounds are reported as $C_cH_hO_oN_nS_s$, where C, H, O, N, and S denote carbon, hydrogen, oxygen, nitrogen, and sulfur, respectively, and the subscripts c,h,o,n, and s indicate the number of atoms of each element. Molecular aromaticity was evaluated using the modified aromaticity index, AI_{mod}.(Koch and Dittmar, 2006) Because heteroatoms (O, N, and S) are treated as potential contributors to π-bond equivalents, AI_{mod} has been considered a useful metric for identifying aromatic structures in complex organic mixtures.(Koch and Dittmar, 2006; Song et al., 2021) Following Koch and Dittmar (2006), AI_{mod} was calculated as:

$$AI_{mod}=\frac{1+c-0.5o-s-0.5h}{c-0.5o-s-n} \quad (1)$$

Values of $AI_{mod} \leq 0$ were set to 0. Molecular formulas were then classified as aromatic ($AI_{mod} \geq 0.5$), olefinic ($0 < AI_{mod} < 0.5$), or aliphatic ($AI_{mod} = 0$).

Text S2. Calculation of lung-deposited surface area.

Lung-deposited surface area (LDSA) was estimated from scanning mobility particle sizer (SMPS) number size distributions by weighting the particle surface area in each size bin by size-dependent respiratory deposition fractions from Hofmann (2011)(Hofmann, 2011). For each SMPS size bin i, the deposited surface area concentration in respiratory region r was calculated as:

$$LDSA_{i,r} = N_i \times \pi \times d_i^2 \times DF_r(d_i), \quad (2)$$

where N_i is the particle number concentration in size bin i (cm^{-3}) from the SMPS number size distribution, d_i is the electrical mobility diameter (converted from nm to μm) corresponding to size bin i, and $DF_r(d_i)$ is the size-dependent deposition fraction (dimensionless) for respiratory region r evaluated at d_i. Under the spherical-particle assumption, $\pi \times d_i^2$ represents the surface area of an equivalent sphere with diameter d_i, so $LDSA_{i,r}$ has units of $\mu m^2\ cm^{-3}$. Regional LDSA was obtained by summing across all bins,

$$LDSA_r = \sum_i N_i \times \pi \times d_i^2 \times DF_r(d_i), \quad (3)$$

and intrathoracic LDSA was calculated by combining tracheobronchial (Tb) and alveolar (Al) deposition fractions,

$$LDSA_{Tb+Al} = \sum_i N_i \times \pi \times d_i^2 \times [DF_{Tb}(d_i) + DF_{Al}(d_i)], \quad (4)$$

the size-dependent deposition fractions $DF_{Tb}(d_i)$ and $DF_{Al}(d_i)$ were taken from the parameterized regional deposition curves reported by Hofmann (2011)(Hofmann, 2011), which are based on the ICRP human respiratory tract model for nose breathing under light activity (ventilation rate 1.2 $m^3\ h^{-1}$). Because the SMPS reports electrical mobility diameter, $d_i$was used as a proxy for particle diameter in both the surface-area term and the deposition weighting. This approximation is most appropriate for near-spherical particles, for which mobility diameter approximates physical diameter; for irregular particles or agglomerates, mobility diameter may differ from the diameter of a sphere having the same external surface area, introducing uncertainty in absolute LDSA. Deposition fractions also depend on breathing route and activity level and may be influenced by hygroscopic growth in the humid respiratory tract. Accordingly, LDSA is used here primarily for relative comparisons across sources and treatments under a consistent set of assumptions rather than as individualized dosimetry.

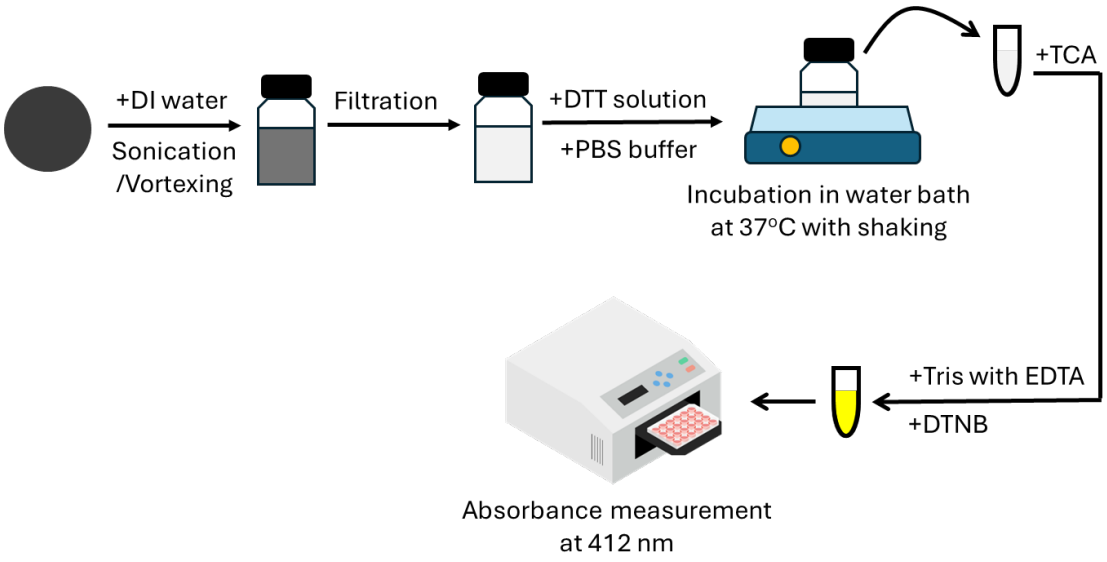

Figure S1. Schematic of the acellular DTT assay. Particle extracts were incubated with DTT in PBS at 37 °C, quenched with TCA, and the remaining DTT was determined by reaction with DTNB (Tris–EDTA) via the absorbance of TNB at 412 nm.

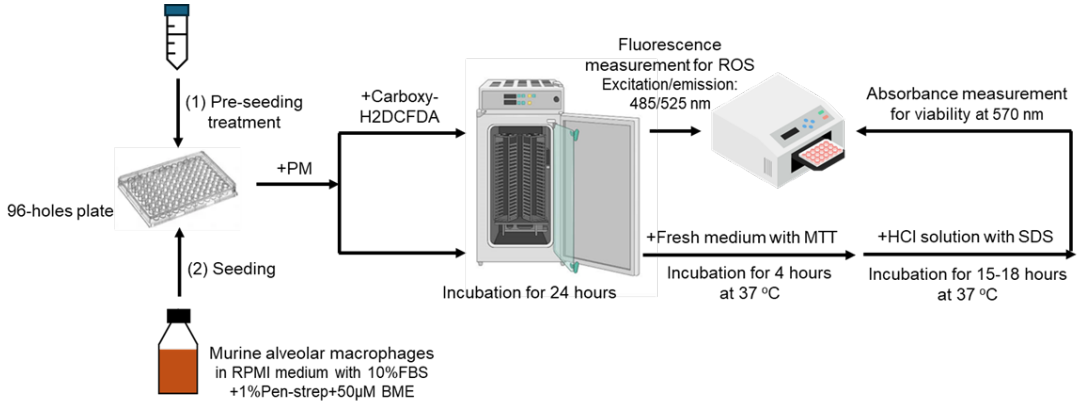

Figure S2. Schematic of the macrophage-based DCFH assay (carboxy-H2DCFDA) for intracellular oxidative-stress response and the accompanying MTT viability assay.

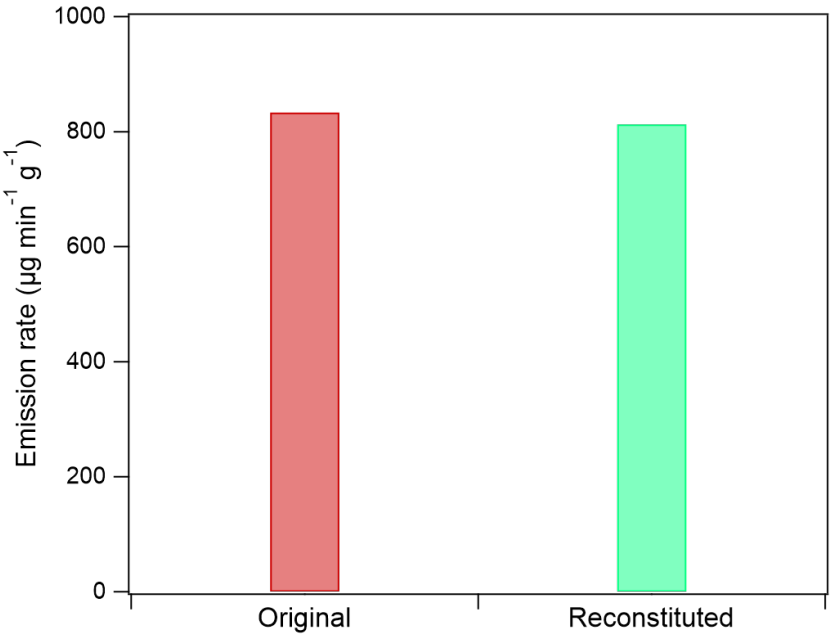

Figure S3. Particle mass emission rate for Bakhoor Type 1 and a hexane-soluble fraction (HSF)-recombined sample prepared by recombining the HSF with the wood residue.

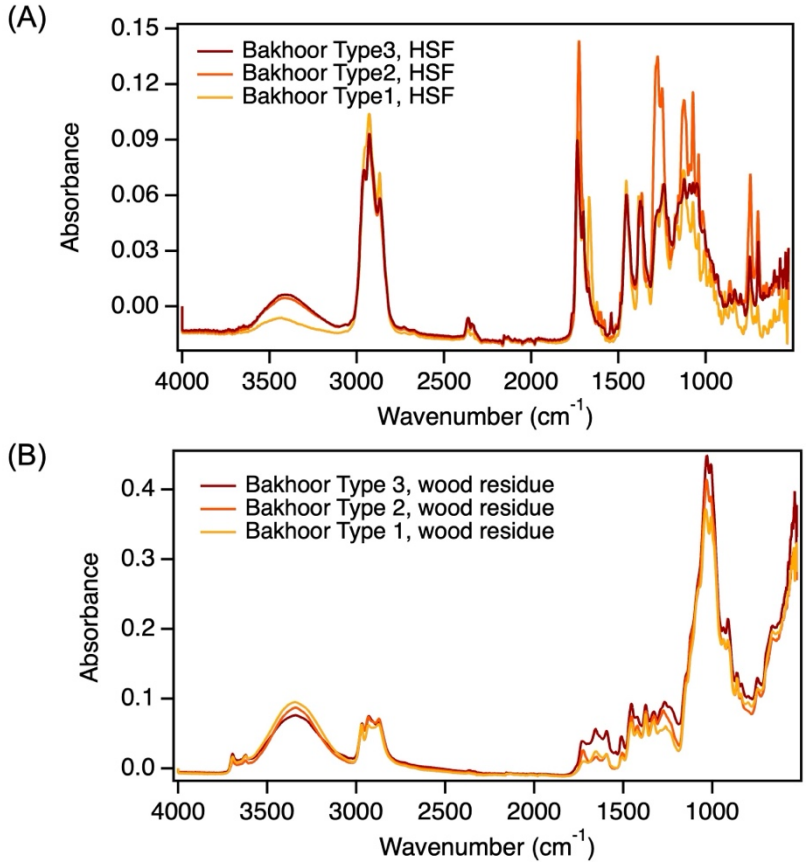

Figure S4. ATR-FTIR absorbance spectra of (A) the hexane-soluble fraction (HSF) and (B) the wood residue for Bakhoor Types 1-3.

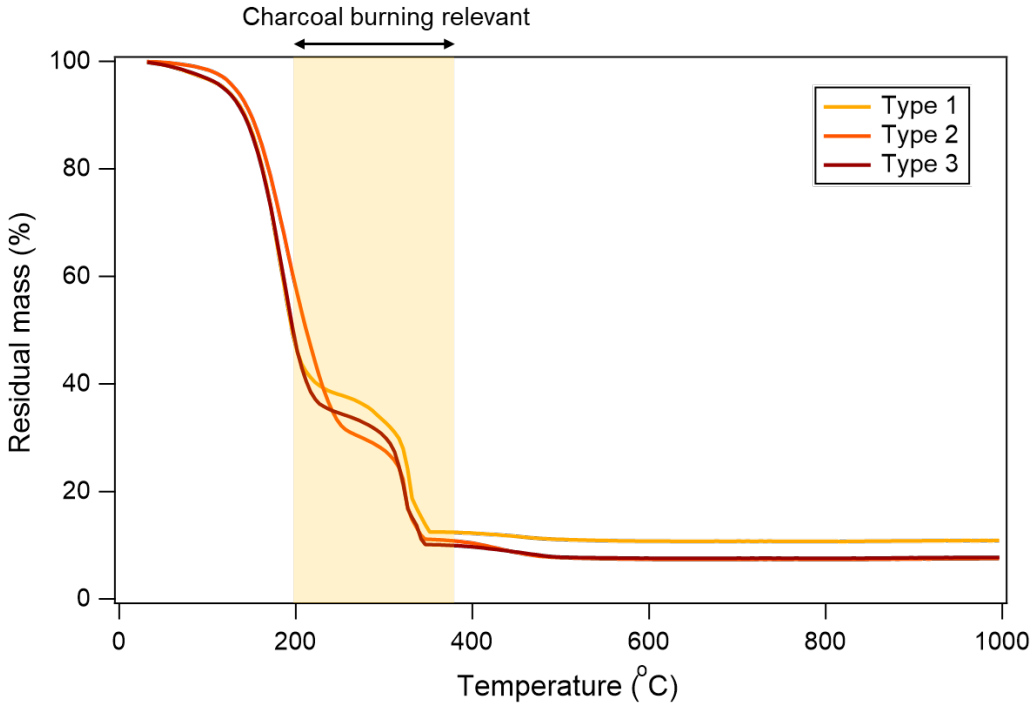

Figure S5. Thermogravimetric analysis of Bakhoor showing residual mass at different temperatures. The heating rate was 20 °C min^{-1}, starting from room temperature. The highlighted region corresponds to the temperature range relevant to charcoal burning.

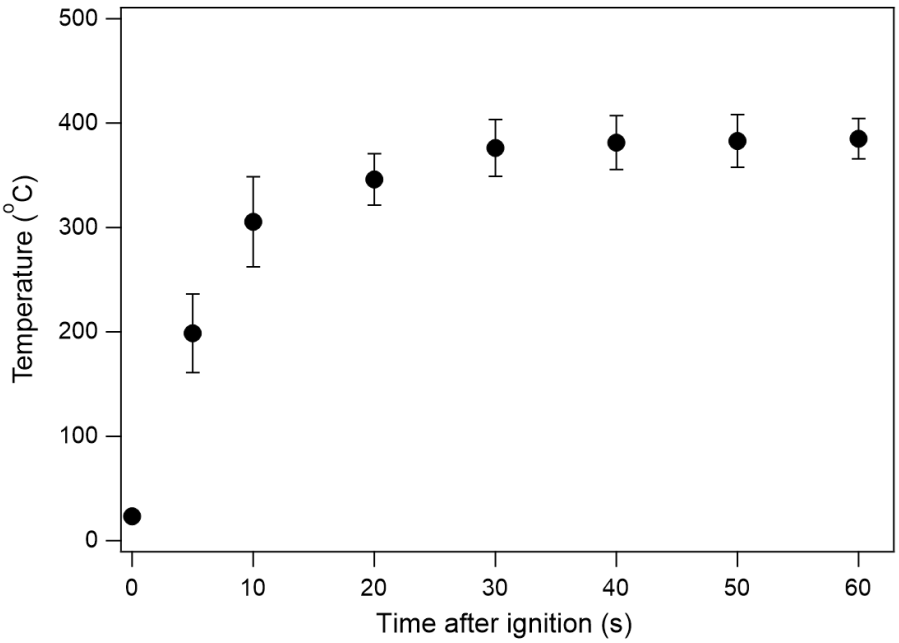

Figure S6. Charcoal temperature as a function of time after ignition. Points show the mean; error bars represent ±1 standard deviation across replicate measurements.

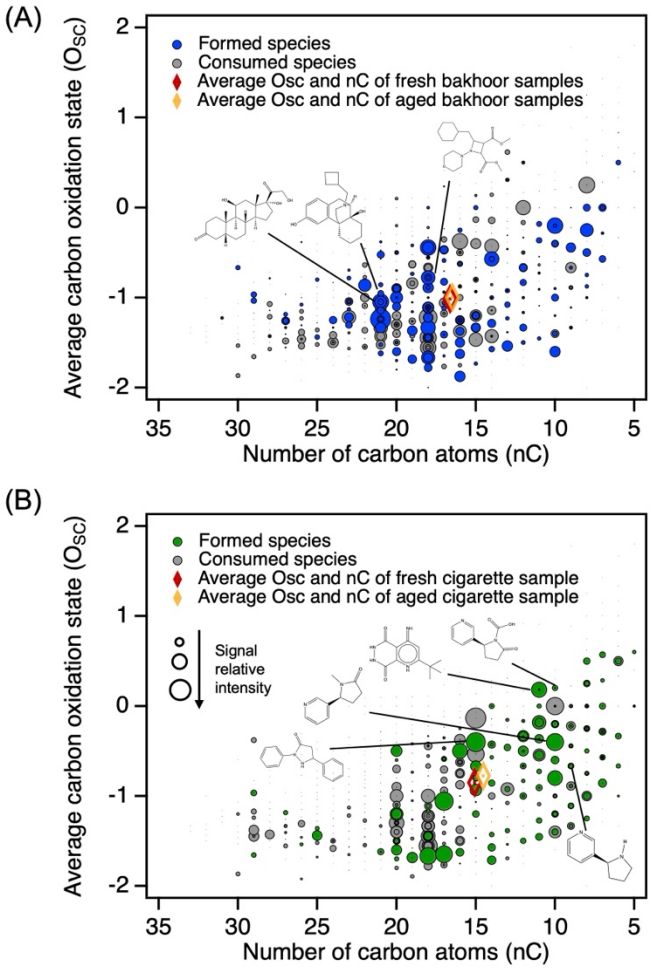

Figure S7. Average carbon oxidation state (OSc) versus number of carbon atoms (nC) for molecular formulas detected in particle extracts before and after O_3 exposure for (A) Bakhoor burning and (B) sidestream cigarette smoke. Colored circles denote formulas with increased signal (formed) after O_3 exposure, and gray circles denote formulas with decreased signal (consumed). Symbol size scales with relative signal intensity, and diamonds indicate sample-average OSc and nC for fresh and O_3-aged samples.

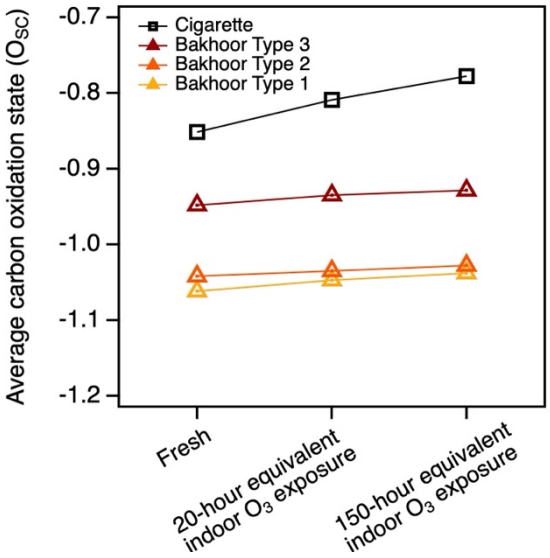

Figure S8. Sample-average carbon oxidation state (OSc) for fresh and O_3-aged (20 h and 150 h equivalent indoor O_3 exposures) particle extracts from Bakhoor burning (Types 1–3) and smoldering sidestream cigarette smoke. Lines are shown to guide the eye.

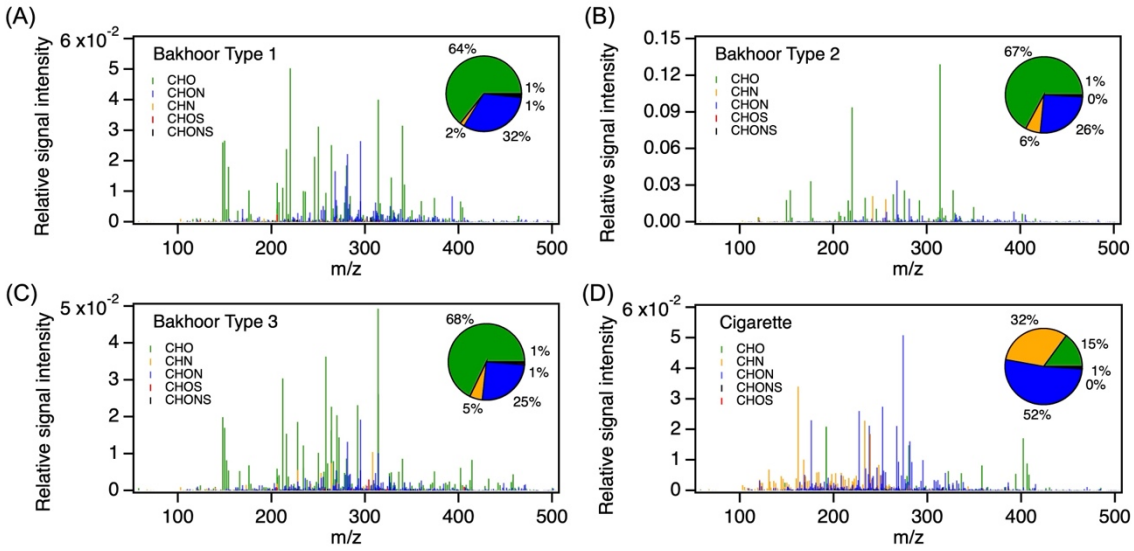

Figure S9. Mass spectra of fresh particle extracts from Bakhoor burning (Types 1-3) and cigarette smoke particles. Colored sticks denote elemental formula classes (CHO, CHON, CHN, CHOS, CHONS), and pie chart insets show the fractional contribution of each class to the total signal intensity.

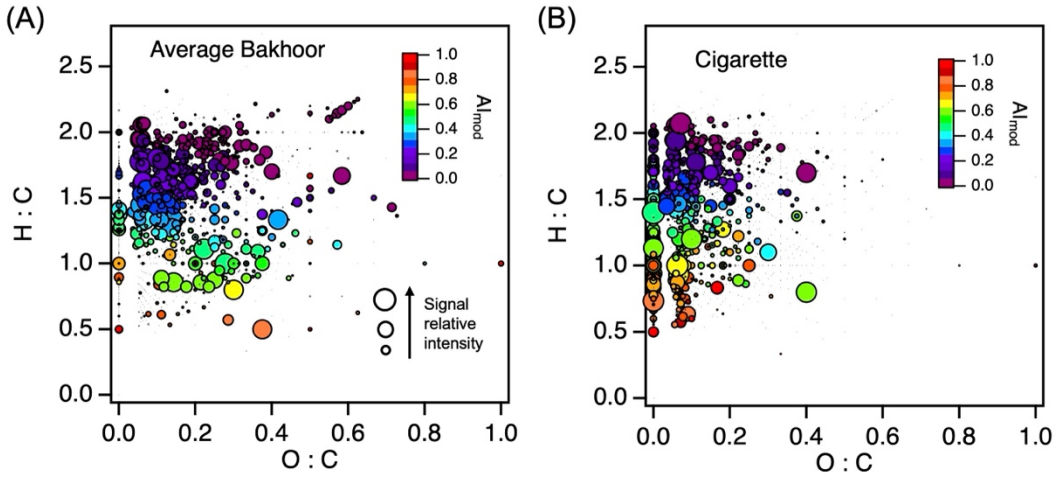

Figure S10. Van Krevelen diagrams (H:C vs O:C) for molecular formulas assigned in particle extracts from (A) Bakhoor burning (mean of Types 1–3) and (B) sidestream cigarette smoke particles. Marker color denotes the modified aromaticity index (AI_{mod}), and marker size scales with relative signal intensity.

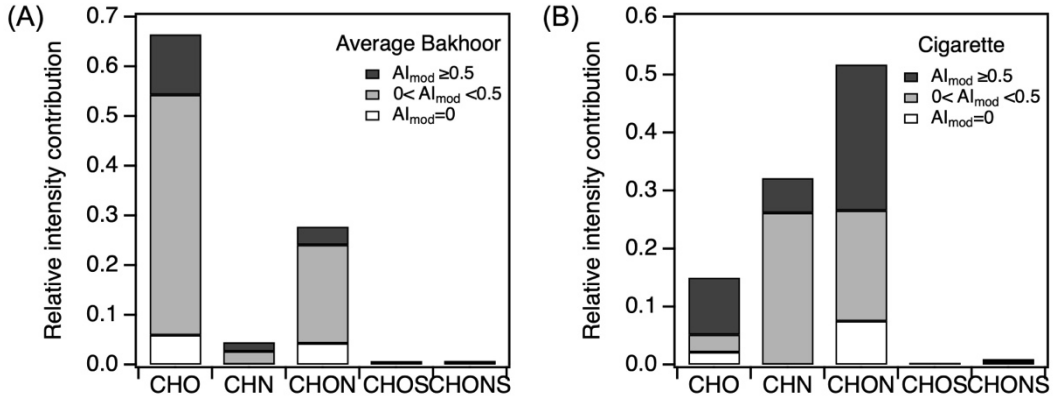

Figure S11. Fractional contributions (by summed relative signal intensity) of molecular formulas in each elemental class (CHO, CHN, CHON, CHOS, CHONS), partitioned by modified aromaticity index (AI_{mod}) for (A) Bakhoor burning particles (average of Types 1–3) and (B) sidestream cigarette smoke particles. Stacked segments denote $AI_{mod} = 0$, $0 < AI_{mod} < 0.5$, and $AI_{mod} \geq 0.5$.

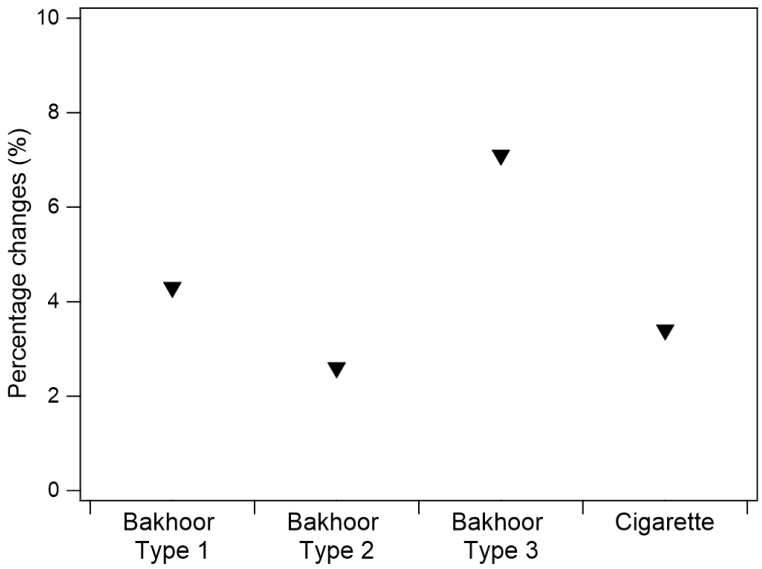

Figure S12. Percentage changes in OP_{DTTm} after Chelex treatment of water extracts from Bakhoor burning particles and sidestream cigarette smoke particles.

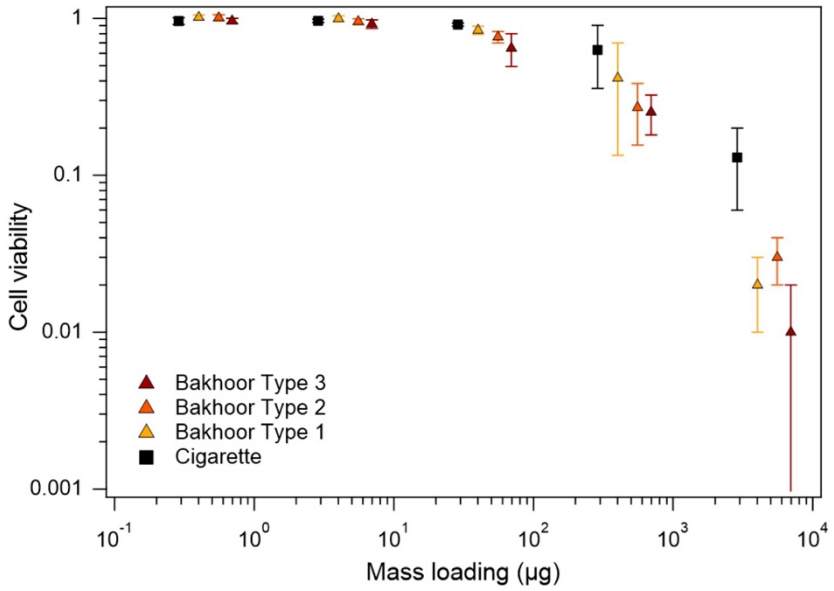

Figure S13. MTT-based cell viability as a function of particle mass loading for Bakhoor burning particles and cigarette smoke particles.

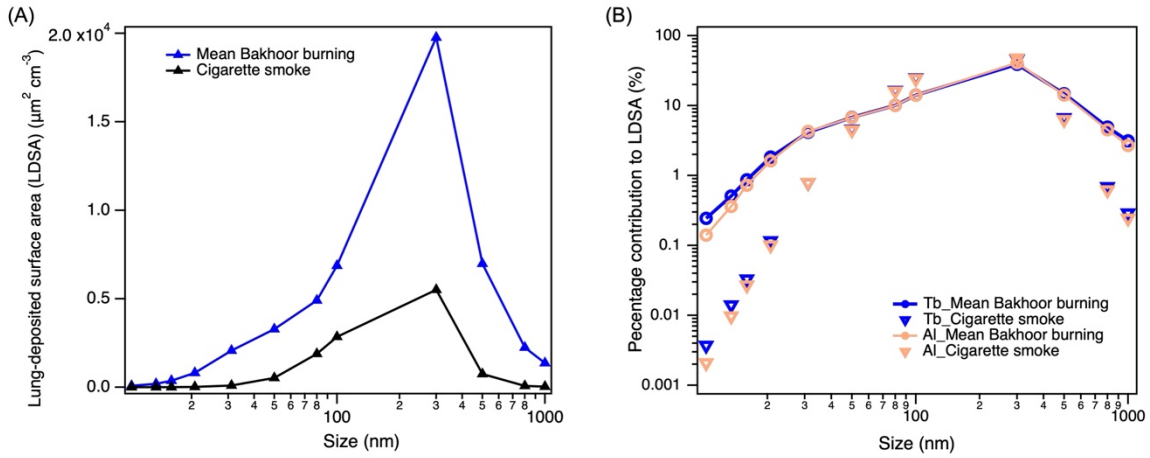

Figure S14. (A) Lung-deposited surface area (LDSA) for particles emitted from Bakhoor burning and sidestream cigarette smoke. (B) Size-resolved contributions of Bakhoor-burning and sidestream cigarette smoke particles to total LDSA in the tracheobronchial (Tb) and alveolar (Al) regions of the human respiratory system.

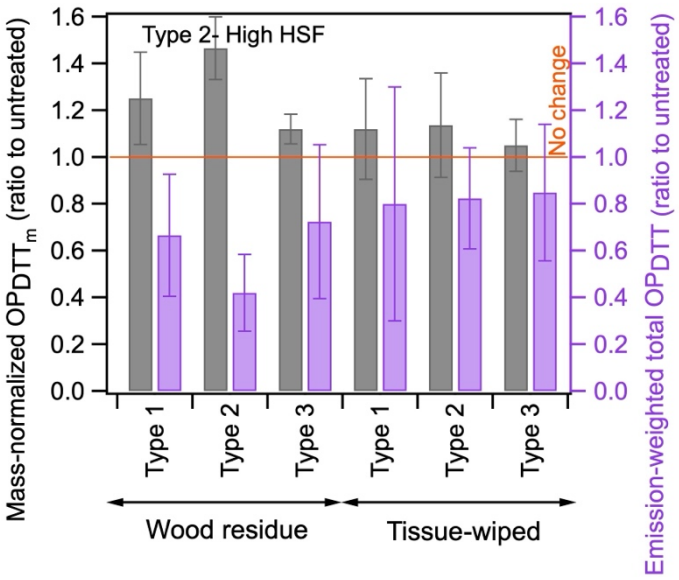

Figure S15. Ratios of DTT-based oxidative potential for particles emitted from wood residue and tissue-wiped Bakhoor relative to the corresponding untreated Bakhoor (Types 1-3). Gray bars (left axis) show the particle mass-normalized DTT consumption rate, OP_{DTTm}; purple bars (right axis) show emission-weighted total OP_{DTT} (OP_{DTTm} multiplied by the particle mass emission rate). The horizontal line indicates unity (no change). Error bars denote 1 standard deviation.

References

Hofmann, W.: Modelling inhaled particle deposition in the human lung—A review, Journal of Aerosol Science, 42, 693-724, 2011.

Koch, B. P. and Dittmar, T.: From mass to structure: An aromaticity index for high-resolution mass data of natural organic matter, Rapid communications in mass spectrometry, 20, 926-932, 2006.

Song, J., Li, M., Zou, C., Cao, T., Fan, X., et al.: Molecular characterization of nitrogen-containing compounds in humic-like substances emitted from biomass burning and coal combustion, Environmental Science & Technology, 56, 119-130, 2021.